

Strong lensing by DHOST black holes

Javier Chagoya^a, C. Ortiz^a, Benito Rodríguez^a, Armando A. Roque^b

^aUnidad Académica de Física, Universidad Autónoma de Zacatecas, 98060, México.

^bDepartamento de Física, Universidad de Guanajuato, 37150 León, Guanajuato, México.

Abstract. The deflection of light in the strong field limit is an important test for alternative theories of gravity. However, solutions for the metric that allow for analytic computations are not always available. We implement a hybrid analytic-numerical approximation to determine the deflection angle in static, spherically symmetric spacetimes. We apply this to a set of numerical black hole solutions within the class of theories known as Degenerate Higher Order Scalar-tensor Theories. Comparing our results to a more time consuming full numerical integration, we find that we can accurately describe the deflection angle for light rays passing at arbitrary distances from the photon sphere with a combination of two analytic-numerical approximations. Furthermore, we find a range of parameters where our DHOST black holes predict strong lensing effects whose size is comparable with the uncertainty in the properties of the supermassive black hole in M87 reported by the Event Horizon Telescope, showing that strong lensing is a viable alternative to put constraints on these models.

1. Introduction

The gravitational deflection of light is one of the most studied predictions of the theory of General Relativity (GR). This effect has been observed in several scenarios, from our Solar System to massive clusters of galaxies (see [1] for a review). In many cases, a weak field approximation to gravitational deflection is enough to explain the existing phenomenology and obtain important information about the theory of gravity. For instance, post-Newtonian studies based on the weak deflection of light by the Sun show that the GR prediction is accurate up to a relative error $\sim 10^{-4}$ [2], forcing any other theory of gravity to satisfy the same constraint. For more complex systems, such as clusters of galaxies, the weak lensing theory based on the assumption that the deflection angle is small has been used to analyse the validity of different theories of gravity on cosmological scales [3, 4].

The deflection of light due to strong gravitational fields has also been studied for a long time. In 1959, Darwin obtained an exact expression for the deflection angle of light in a Schwarzschild spacetime [5], and some years later further analysis of black

hole lenses were presented, in what could be considered as the beginning of black hole imaging [6, 7]. Interest in strong lensing received a boost when the possibility of obtaining an image of the area near a black hole was first discussed [8, 9]. Recently, the Event Horizon Telescope (EHT) imaged the structure around a supermassive black hole [10], finding a ring structure with an angular diameter of $42 \pm 3 \mu\text{as}$. This offers a way not only to investigate the region around a black hole, but also to use this information to test alternative theories of gravity in the strong field regime, imposing constraints on these theories that are complementary to those obtained under weak field approximations. This has motivated several studies of the strong deflection angle in spacetimes predicted by modifications to GR (see, e.g., [11, 12, 13, 14, 15]). These studies rely on the existence of an analytical solution for the metric in the modified theory of gravity under consideration[‡]. The deflection angle is then studied under some approximations, in particular, Bozza [17] introduced a method that separates and carefully describes the divergent part of the deflection angle at the photon sphere from the regular part. For a Schwarzschild black hole, Bozza’s method can be compared with the exact result, giving a discrepancy in the deflection angle of about 0.06%. For other black holes, the results of the approximation are sometimes compared with the full numerical results, also giving good agreement near the photon sphere. By construction, Bozza’s approximation is valid only at very short distances from the photon sphere. For larger distances, a different approximation that is equally capable of handling any spherically symmetric, static, asymptotically flat spacetime was presented in [18], where it was also shown that this approximation is in good agreement with exact results for Schwarzschild and Reissner-Nördstrom black holes almost up to the photon sphere.

In this work we use the approximations mentioned above to study the deflection angle in a particular model of modified gravity. Specifically, we use a numerical solution for a static, spherically symmetric spacetime in a scalar-tensor theory that belongs to beyond Horndeski [19, 20], a generalization of Horndeski gravity [21], which is the most general scalar-tensor theory with equations of motion that are explicitly second order, thus avoiding the propagation of Ostrogradski degrees of freedom [22]. In beyond Horndeski and further generalizations, known as *Degenerate Higher Order Scalar-tensor theories* (DHOST) [23, 24] or *Extended Scalar-tensor Theories* (EST) [25], higher order equations of motion are allowed as long as the Hessian matrix of the system is degenerate, thus introducing constraints that prevent the propagation of the Ostrogradski ghost.

Scalar-tensor modifications of gravity are generally motivated by their applications to cosmology (see [26] for a review). On the other hand, the phenomenology of these theories in astrophysical scenarios needs to be studied as well in order to evaluate their physical viability, this has been explored in several works considering the properties of black holes and relativistic stars in scalar-tensor theories [27, 28, 29, 30, 31, 32, 33]. Findings are diverse, depending on the specific model under consideration, black hole solutions may or may not be the same as in GR, either exactly or asymptotically. An

[‡] There are exceptions, in [16] a numerical computation is presented for the deflection angle in higher derivative gravity theories, however, the method is tested against weak deflection data.

important restriction on the models that can be considered is that the propagation speed of gravitational waves, c_{GW} , is within 10^{-16} of the speed of light [34], this is derived from the detection of gravitational waves with an electromagnetic counterpart made by LIGO, VIRGO and several other observatories [35]. Within Horndeski, only the quadratic and cubic sectors predict $c_{GW}/c = 1$. However, when beyond Horndeski is included, this condition can be satisfied by particular combinations of quartic and quintic Lagrangians (e.g. [36]).

In this work we use one of the beyond Horndeski models that is compatible with $c_{GW}/c = 1$. The static, spherically symmetric vacuum solutions of this model, studied in [32], are not exactly Schwarzschild, making it interesting to explore their observational signatures in the strong field regime. Furthermore, since these models contain an angular deficit, we discuss the constraints that can be imposed in the weak deflection limit. Not less importantly, the solutions that we use are known in analytic form only asymptotically, and numerically for the complete range of the radial coordinate, offering a non-trivial situation where we can demonstrate that the methods proposed in [17, 18] for computing (strong) deflection angles in spherically symmetric spacetimes can be implemented numerically, and the results are consistent with a full numerical computation of the deflection angle.

This work is organised as follows. In Sec. 2 we give an overview of beyond Horndeski, the particular model that we use, and the black hole solutions of this model. In Sec. 3 we outline the strong deflection limit and related lensing observables following the method of [17]. In Sec. 4 we perform a numerical implementation of this method in order to compute the strong deflection angle in the spacetimes that we are interested in. The results of this section are applied in Sec. 5 to compute lensing observables for two supermassive black hole candidates: Sagittarius A* and M87; in particular, we obtain the asymptotic position and separation of the lensed images. In Sec. 6 we discuss the deflection angle far from the photon sphere, using a numerical implementation of [18], and we discuss how well the methods that we use approximate the results of full numerical computations. Sec. 7 is devoted to discussion and concluding remarks.

2. Black hole solutions in beyond Horndeski

The Horndeski Lagrangians [21] describe the most general scalar-tensor theory with equations of motion that are explicitly second order, thus guaranteeing that the system is free of Ostrogradsky instabilities [22]. Let ϕ be the scalar field, the Horndeski Lagrangians are given by [37, 38]

$$\begin{aligned}\mathcal{L}_2 &= G_2, \\ \mathcal{L}_3 &= G_3[\Phi], \\ \mathcal{L}_4 &= G_4 R + G_{4,X} \{[\Phi]^2 - [\Phi^2]\}, \\ \mathcal{L}_5 &= G_5 G_{\mu\nu} \Phi^{\mu\nu} - \frac{1}{6} G_{5,X} \{[\Phi]^3 - 3[\Phi][\Phi^2] + 2[\Phi^3]\},\end{aligned}\tag{1}$$

where Φ is a matrix with components $\nabla^\mu \nabla_\nu \phi$, $G_{i,X}$ denotes derivatives of the functions G_i with respect to X , and

$$X = -\frac{1}{2} \partial_\mu \phi \partial^\mu \phi, \quad [\Phi^n] = \text{tr}(\Phi^n), \quad \langle \Phi \rangle = \partial^\mu \phi \partial_\mu \partial_\nu \phi \partial^\nu \phi. \quad (2)$$

Assuming that the action is invariant under the shift $\phi \rightarrow \phi + \text{const}$, G_i are arbitrary functions only of X . The condition that the equations of motion are explicitly second order can be relaxed without introducing Ostrogradsky ghosts as long as the Hessian matrix of the system, obtained by taking second derivatives of the Lagrangian with respect to velocities, is degenerate. In this case it is said that the Lagrangian is degenerate. These generalizations were first introduced as *Degenerate Higher Order Scalar-tensor Theories* (DHOST) [23] or *Extender Scalar-tensor Theories* [25] for Lagrangians that depend quadratically on second derivatives of a scalar field, and then generalized in [24] for cubic dependence on second derivatives. The first realisations of DHOST theories were given in [19, 20], and are known as *beyond Horndeski* or GLPV Lagrangians.

Astrophysical systems in DHOST theories provide a way for testing these models of gravity. One feature of these theories is the presence of *screening mechanisms* that are usually very efficient outside matter sources, but can be broken in the interior region. For instance, in different sectors of the theory, it has been shown that outside the source the metric behaves qualitatively as the standard solutions of GR [39], that it is exactly Schwarzschild-de-Sitter [28], or that it is exactly Schwarzschild [33]. The breaking of the screening mechanism inside astrophysical bodies has been studied in these same references (see also [40]). The fact that the screening works well outside the matter source makes it more difficult to devise tests for these theories of gravity using compact objects, but tests using galactic scale systems have been proposed. On the observational side, the detection of gravitational waves from the neutron star merger GW170817 and its associated electromagnetic counterpart GRB170817A [35] put tight constraints on the speed of gravitational waves, that are satisfied by a limited class of DHOST theories. One of the models within this limited sector is given by

$$\mathcal{L}_c = X + \mathcal{L}_4 + \mathcal{L}_4^{bH}, \quad (3)$$

where the quartic beyond Horndeski Lagrangian is

$$\mathcal{L}_4^{bH} = -\frac{1}{2} F_4 \epsilon^{\mu\nu\rho}{}_\sigma \epsilon^{\mu'\nu'\rho'\sigma} \partial_\mu \phi \partial_{\mu'} \phi \Phi_{\nu\nu'} \Phi_{\rho\rho'}, \quad (4)$$

and F_4 is subject to $F_4 = G_{4,X}/X$. After some manipulations, \mathcal{L}_c is reduced to

$$\mathcal{L}_c = X + G_4 R + \frac{G_{4,X}}{X} (\langle \Phi^2 \rangle - \langle \Phi \rangle [\Phi]). \quad (5)$$

Static, spherically symmetric solutions to this model were studied in [32], both for black holes and relativistic stars, with

$$G_4(X) = M_{Pl}^2 + g_4 X, \quad (6)$$

and g_4 a constant with dimensions of inverse mass squared. A feature of these solutions is that the metric acquires a deficit angle as a result of a linear dependence in time of

the scalar field and of the presence of the kinetic term X in the Lagrangian \mathcal{S} . Even if the remaining components of the metric are very similar to GR solutions, the deficit angle signals a breaking of the screening mechanism outside the astrophysical source, and it opens up the possibility for testing this model with phenomenology away from the source. In order to do so, let us present in more detail the black hole solutions to the model (5). The assumptions for the scalar field and metric are

$$\phi = M_{Pl}(\phi_0 t + \phi_1(r)), \quad (7)$$

$$ds^2 = -f(r)dr^2 + h(r)^{-1}dr^2 + s_0^{-1}r^2(d\theta^2 + \sin^2\theta d\varphi^2), \quad (8)$$

where ϕ_0 and s_0 are constant. The form of G_4 and ϕ is such that M_{Pl} factors out of the Lagrangian. The equations of motion fix $s_0 = 1 - 3g_4\phi_0^2$. The functions $f(r)$, $h(r)$ and $\phi_1(r)$ are found asymptotically as

$$f(r) = 1 - \frac{2M}{r} - \frac{4g_4^2\phi_0^2(g_4\phi_0^2 - 2)}{r^2} + \mathcal{O}\left(\frac{1}{r^3}\right), \quad (9a)$$

$$h(r) = 1 - \frac{2M}{r} + \frac{4g_4^2\phi_0^2(1 - g_4\phi_0^2)}{r^2} + \mathcal{O}\left(\frac{1}{r^3}\right), \quad (9b)$$

$$\phi_1'(r) = \phi_0 + \frac{2M\phi_0}{r} + \frac{2\phi_0[2g_4^3\phi_0^4 + (2M^2 - g_4) - 3g_4^2\phi_0^2]}{r^2} + \mathcal{O}\left(\frac{1}{r^3}\right), \quad (9c)$$

where M is an integration constant. Solutions for arbitrary r are obtained numerically, imposing (2) as asymptotic conditions. In Fig. 1 we reproduce a set of solutions presented in [32] for $2M = g_4 = 1$ and different values of ϕ_0 . As ϕ_0 increases, the horizon shrinks until it finally disappears, this defines the range of ϕ_0 that admits regular black hole solutions for a given mass. In the next sections, we present the formalism for studying strong lensing and then we apply it to this set of solutions, first for arbitrary masses in order to analyse the generic properties of the model, and then for two specific astrophysical black holes whose masses and distances are known observationally.

3. Strong deflection limit

Let us briefly review the analytical method that we use as a starting point for our numerical computations. We consider geometries described by the line element^{||}

$$ds^2 = -A(r)dt^2 + B(r)dr^2 + C(r)(d\theta^2 + \sin^2\theta d\varphi^2). \quad (10)$$

A dimensionless variable $x(r)$ is often introduced. If the metric components A, B are asymptotically Schwarzschild, as is the case for the metrics we consider in this work, this variable is naturally defined as $x = r/2M$, where M is the Schwarzschild mass. We

^S The exact Schwarzschild exterior metric found in [33] is for a model that does not include the standard kinetic term.

^{||} The asymptotic conditions $\lim_{r \rightarrow \infty} A = \lim_{r \rightarrow \infty} B = 1$ and $\lim_{r \rightarrow \infty} C = r^2$ are sometimes imposed in order to ensure asymptotic compatibility with the Minkowski metric. In our case, only the first two conditions are true, while $\lim_{r \rightarrow \infty} C = s_0^{-1}r^2$, with s_0 defined in (8). Mathematically, the method we are using works also for this asymptotic condition.

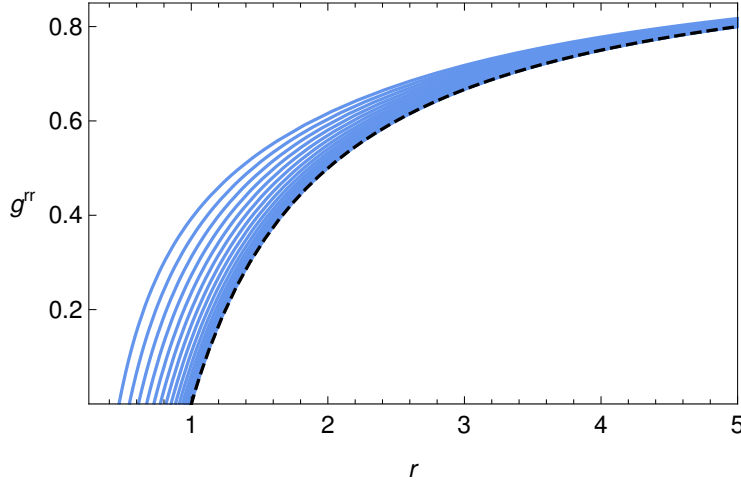


Figure 1. Numerical BH solutions for $2M = g_4 = 1$. The figure shows the metric component g_{rr} in GR (black, dashed line) and in the beyond Horndeski model we are considering, with ϕ_0 spanning between 0.02 and 0.32 (blue, solid lines). The size of the black hole horizon decreases as ϕ_0 increases. The profiles for the metric component g^{tt} , not shown, are similar.

are interested in studying the deflection of light rays passing near the photon sphere, whose radius x_m is given by the outermost solution of

$$\frac{C'(x)}{C(x)} = \frac{A'(x)}{A(x)}, \quad (11)$$

where primes denote derivatives with respect to x . Following the classical computation of [41], it has been shown [11] that the metric (10) predicts that the deflection angle of photons is

$$\begin{aligned} \alpha(x_0) &= 2 \int_{x_0}^{\infty} dx \sqrt{\frac{B(x)}{C(x)} \left[\frac{C(x)A(x_0)}{A(x)C(x_0)} - 1 \right]^{-\frac{1}{2}}} - \pi \\ &\equiv I(x_0) - \pi, \end{aligned} \quad (12)$$

where x_0 is the distance of closest approach of the light ray to the center of the gravitational attraction. In the strong deflection limit, the integral $I(x_0)$ diverges logarithmically [42]. Indeed, it can be separated into a divergent and a regular part,

$$I(x_0) = I_D(x_0) + I_R(x_0). \quad (13)$$

After taking expansions near $x_0 = x_m$, and writing x_0 in terms of its associated impact parameter [17, 42]

$$b(x_0) = \sqrt{\frac{C(x_0)}{A(x_0)}}, \quad (14)$$

the deflection angle can be written as

$$\alpha(\beta) = -c_1 \log \left(\frac{b}{b_c} - 1 \right) + c_2 + \mathcal{O}[(b - b_c) \log(b - b_c)], \quad (15)$$

where b_c is the critical impact parameter, i.e., the impact parameter for a light ray with closest approach distance $x_0 = x_m$. The parameters c_1 and c_2 depend only on x_m – although x_m itself could depend on the parameters of the black hole solution. The divergent part of the integral $I(x_0)$ appears in the deflection angle through the logarithmic term, and its coefficient c_1 is equal to

$$c_1 = \sqrt{\frac{2A_m B_m}{C_m'' A_m - C_m A_m''}}, \quad (16)$$

where a subscript m denotes evaluation at the photon sphere, x_m . The regular part is left explicitly in

$$c_2 = c_1 \log \left[x_m^2 \left(\frac{C_m''}{C_m} - \frac{A_m''}{A_m} \right) \right] + I_R(x_m) - \pi. \quad (17)$$

Notice that I_R takes the photon sphere radius x_m as parameter instead of x_0 , this is because we are in the limit $x_0 \rightarrow x_m$, and the correction terms of order $(b - b_c) \log(b - b_c)$ or higher are all being neglected. In order to avoid integrating up to infinity, it is convenient to introduce a new coordinate z defined by

$$x(z) = \frac{x_m}{1 - z}. \quad (18)$$

In terms of this coordinate, I_R is written as

$$I_R(x_m) = 2x_m \int_0^1 dz \left[\sqrt{\frac{B(z)}{C(z)}} \left(\frac{C(z) A_m}{A(z) C_m} - 1 \right)^{-\frac{1}{2}} \frac{1}{(1 - z)^2} \right] - \frac{c_1}{x_m z}. \quad (19)$$

The last term comes from the definition of I_R , which implies subtracting from $I(x_0)$ the part that integrates to a logarithmic divergence [17].

Summing up, the method described above allows us to compute the deflection angle by performing the following steps:

- i. Use Eq. (11) to determine x_m .
- ii. Obtain c_1 from Eq. (16).
- iii. Compute I_R from Eq. (19).
- iv. Compute c_2 from Eq. (17).

This method has been used for studying the deflection angle of several black holes, such as Schwarzschild and Reissner-Nördstrom [17, 42], but it has also been used for a particular exact solution of Horndeski gravity [14], as well as for the Janis-Newman-Winicour naked singularity in GR minimally coupled to a massless scalar field [11], and for a Schwarzschild black hole pierced by a cosmic string (which induces a deficit angle) [43], to mention a few examples. Before obtaining results for the deflection angle, let us define the lensing observables that we are interested in.

3.1. Lensing observables

We start with the lens equation in the situation where the source and lens are almost perfectly aligned [44],

$$\beta = \theta - \frac{D_{LS}}{D_{OS}} \Delta\alpha_n, \quad (20)$$

where β and θ are, respectively, the angles between the observer and the source and between the observer and the image, both measured with respect to the optical axis, D_{LS} is the distance between the lens and the source plane measured along the optical axis, D_{OS} is the distance between the observer and the source plane, also measured along the optical axis, and $\alpha = 2\pi n + \Delta\alpha_n$. This last relation expresses the fact that, in the strong gravity regime, the high alignment between lens and source does not imply that the deflection angle is small, instead, light rays may complete n loops around the lens and then travel towards the observer with an effective deflection angle $|\Delta\alpha_n| \ll 1$. The deflection angle Eq. (15) can be written in terms of θ by noticing that, by assumption, θ is a small angle, and can therefore be approximated as $\theta \approx b/D_{OL}$, thus

$$\alpha(\theta) = -c_1 \log \left(\frac{\theta D_{OL}}{b_c} - 1 \right) + c_2 + \dots \quad (21)$$

As described in [44], the effective angle $\Delta\alpha_n$ can be translated to a small change in θ by expanding $\alpha(\theta)$ angle around the value θ_n^0 such that $\alpha(\theta_n^0) = 2\pi n$, i.e.,

$$\Delta\theta_n = \theta - \theta_n^0, \quad (22)$$

with

$$\begin{aligned} \theta_n^0 &= \frac{b_c}{D_{OL}} (1 + e_n), \\ e_n &= \exp \left(\frac{c_2 - 2n\pi}{c_1} \right). \end{aligned} \quad (23)$$

Notice that θ_n decreases exponentially as n increases. Taylor expanding $\alpha(\theta)$ near θ_n^0 and substituting the previous result, we find

$$\Delta\alpha_n = -\frac{c_1 D_{OL}}{b_c e_n} \Delta\theta_n. \quad (24)$$

Using this result, the lens equation (20) becomes

$$\beta = \theta + \frac{D_{LS}}{D_{OS}} \frac{c_1 D_{OL}}{b_c e_n} \Delta\theta_n. \quad (25)$$

This can be used to compute the magnification,

$$\mu_n = \left. \frac{1}{\frac{\beta}{\theta} \frac{\partial \beta}{\partial \theta}} \right|_{\theta} \approx \left. \frac{1}{\frac{\beta}{\theta} \frac{\partial \beta}{\partial \theta}} \right|_{\theta_n^0}, \quad (26)$$

where we are neglecting the correction term $\Delta\theta_n$. After a few manipulations, this becomes

$$\mu_n = e_n \frac{b_c^2 (1 + e_n) D_{OS}}{c_1 \beta D_{OL}^2 D_{LS}}. \quad (27)$$

Instead of working with individual magnifications, it is more convenient to define

$$r = \mu_1 \left(\sum_{n=2}^{\infty} \mu_n \right)^{-1}, \quad (28)$$

i.e., the ratio between the magnification of the outermost image, located at θ_1 , and the sum of the magnification of all the other images, whose position quickly approaches θ_∞ , given by the limit as $n \rightarrow \infty$ of Eq. (23). The denominator in r can be summed exactly as a geometric series, and the result can be approximated under the assumption that c_1 and c_2 are of order unity, which is known to hold for Schwarzschild and can be verified for the metrics that we consider later on. The final, approximated result is simply

$$r = e^{2\pi/c_1}. \quad (29)$$

Thus, obtaining r is straightforward from the results described in the previous subsection. In order to agree with the conventions used in the literature, we will report the values of

$$r_m = 2.5 \log_{10} r.$$

The second observable that we report is the separation between the first image and the others, given by

$$s = \theta_1 - \theta_\infty \approx \theta_1^0 - \theta_\infty. \quad (30)$$

Under the same assumptions that we made for r , this is reduced to

$$s \approx \theta_\infty \exp\left(\frac{c_2 - 2\pi}{c_1}\right) = \frac{b_c}{D_{OL}} \exp\left(\frac{c_2 - 2\pi}{c_1}\right). \quad (31)$$

The observables r and s are completely determined by c_1 , c_2 , b_c and D_{OL} . This last quantity is fixed by observations, while the other three depend on the parameters that appear in the black hole solution under consideration, i.e., on the mass – also observed – and on the parameters that appear as a result of considering alternative models of gravity. In the next section we compute quantities that do not depend on D_{OL} for several numerical black hole solutions of beyond Horndeski, while the ones that do depend on D_{OL} are presented in Sec. 5.

4. Numerical implementation and results

Let us study the deflection angle in the strong gravity regime for the solutions of beyond Horndeski presented in Fig. 1. Since these solutions are numerical, our results here are also numerical. However, the limit $\phi_0 \rightarrow 0$ recovers the Schwarzschild solution, thus it can be used as a reference to validate our results. Although not strictly necessary, it is convenient to introduce variables such that the black hole solution does not depend explicitly on the Schwarzschild mass M . This is achieved by using $2M$ as unit of distance, i.e., introducing $x = r/2M$, and redefining the constants that appear in the asymptotic solutions (which act as boundary conditions) in order to absorb any factor of M . The appropriate redefinitions for eqs. (2) are $g_4 = 4M^2 \tilde{g}_4$ and $\phi_0 = \tilde{\phi}_0/2M$. One

should keep in mind that this redefinition is only for numerical convenience, and it is not well justified from a theoretical point of view, for instance, \tilde{g}_4 cannot be interpreted as parameters of the model since now it depends on the mass scale of the system under consideration. It is convenient to keep in mind that $g_4\phi_0^2 = \tilde{g}_4\tilde{\phi}_0^2$.

Using the redefined quantities $x, \tilde{g}_4, \tilde{\phi}_0$, the asymptotic metric takes the form

$$f(x) = 1 - \frac{1}{x} - \frac{4\tilde{g}_4^2\tilde{\phi}_0^2(\tilde{g}_4\tilde{\phi}_0^2 - 2)}{x^2} + \mathcal{O}\left(\frac{1}{x^3}\right), \quad (32a)$$

$$h(x) = 1 - \frac{1}{x} + \frac{4\tilde{g}_4^2\tilde{\phi}_0^2(1 - \tilde{g}_4\tilde{\phi}_0^2)}{x^2} + \mathcal{O}\left(\frac{1}{x^3}\right). \quad (32b)$$

Strictly speaking, one should redefine r also in the line element. This would introduce a global factor of $4M^2$ both in the radial and in the angular components of the redefined metric, these factors are not explicitly considered in the literature, but are correctly accounted for when reporting the impact parameter, Eq. (14), as $b/2M$ instead of simply b (see, e.g., [17]). The global factors of $4M^2$ cancel out in all the other quantities introduced in the previous sections. Having clarified this, we proceed to apply the formalism of Sec. 3, with the identifications

$$A(x) = f(x), \quad B(x) = 1/h(x), \quad C(x) = (1 - 3\tilde{g}_4\tilde{\phi}_0^2)^{-1}x^2. \quad (33)$$

Let us describe the numerical implementation of the steps i-iv enumerated in Sec. 3. For concreteness and numerical convenience, we make $\tilde{g}_4 = 1$, and we vary $\tilde{\phi}_0$ in the range $0 < \tilde{\phi}_0 \leq 0.32$ where regular black hole solutions exist.

- i. Use Eq. (11) to determine x_m . We use a numerical root finder in the range $x_h < x < 2$, where x_h is the size of the horizon obtained from the numerical solutions for each value of $\tilde{\phi}_0$. For $\tilde{\phi}_0 \rightarrow 0$, x_h recovers the horizon of a Schwarzschild black hole, $x_h = 1$, and it decreases as $\tilde{\phi}_0$ increases. Similarly, x_m approaches its Schwarzschild value, $x_m = 3/2x_h = 3/2$ for small $\tilde{\phi}_0$, and it decreases as $\tilde{\phi}_0$ increases. It is interesting to note that the ratio between the photon sphere and the horizon, x_m/x_h , remains nearly constant as $\tilde{\phi}_0$ varies: the relative differences $1 - x_m/x_h$ are of order 10^{-3} , i.e., for these black holes the photon sphere is relatively at the same distance from the horizon than it is for a Schwarzschild black hole. Once x_m is known, it is straightforward to compute also the critical impact parameter $b_c = b(x_m)$ using Eq. (15). Studying the relation between b_c and x_h we find that their ratio increases with $\tilde{\phi}_0$: for the black holes that we are considering, the horizon is smaller than it is for a Schwarzschild black hole, but they capture photons over a larger radius in relation to the size of their horizon. This is shown in Fig. 2.
- ii. Obtain c_1 from Eq. (16). Once we have x_m , it is straightforward to evaluate the argument of Eq. (16) as long as an interpolation of the numerical solutions and their derivatives at x_m are known. If that is not the case, we have verified that a cubic polynomial interpolation on a set of data points spaced by $\Delta x = 0.01$ is enough to get values of c_1 with a relative difference of order 10^{-4} with respect to

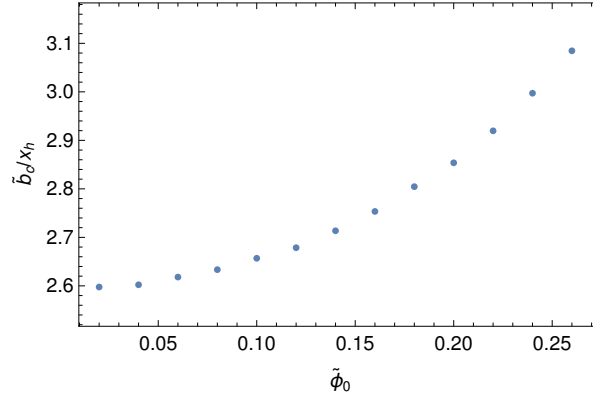


Figure 2. Critical impact parameter, $\tilde{b}_c = b_c/2M$, divided over the horizon of each solution, for $0 < \tilde{\phi}_0 < 0.26$.

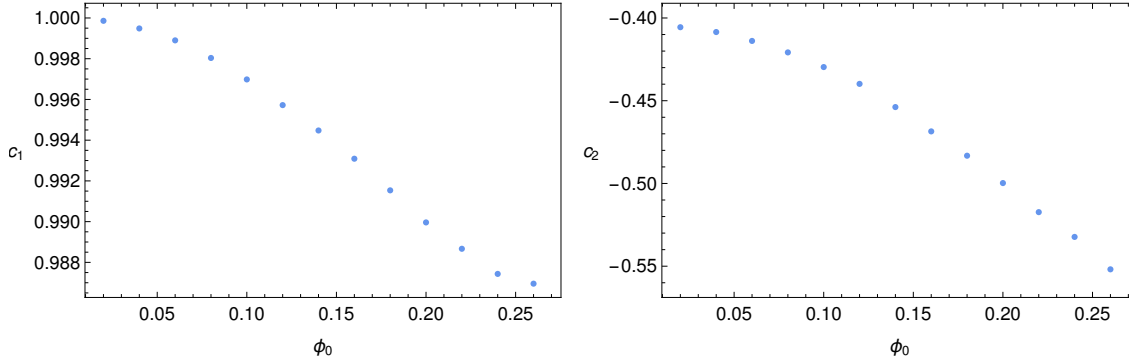


Figure 3. Parameters c_1 and c_2 that determine the strong deflection limit in Bozza's approximation, for $0 \leq \tilde{\phi}_0 \leq 0.24$. Notice that the relative change with respect to Schwarzschild ($\tilde{\phi}_0 = 0$) is much smaller in c_1 than in c_2 .

those obtained for a more precise solution with $\Delta x = 0.0005$. Our results for c_1 are displayed in the left panel of Fig. 3. We see a small relative change, around 10^{-2} , from the Schwarzschild value $c_1 = 1$. As we notice below, this change is also small in comparison to the change in c_2 .

- iii. Compute I_R from Eq. (19). For this step it is convenient to write the solutions for the metric in terms of the variable z defined in Eq. (18). It is important to notice that this redefinition is different for every solution since it depends on the value of x_m . Nevertheless, it has the advantage of reducing the range of integration to $0 \leq z \leq 1$. Numerically we cannot use these exact limits since at $z = 0$ the argument of the integral diverges and $z \rightarrow 1$ implies $x \rightarrow \infty$. Instead, we use $z = 0.00001$ and $z = 0.997$. These limits ensure that the result of the integral does not change by more than 10^{-3} if the integration range is extended. One should be careful with changing the upper limit because of the inverse relation between x and $1 - z$: if z was very close to 1 we would need to know the numerical solution up to a very large value of x , for instance, $z = 0.998$ translates to $x > 500$ for all of the values of x_m that we find, and $z = 0.999$ translates to $x > 1000$. The value that

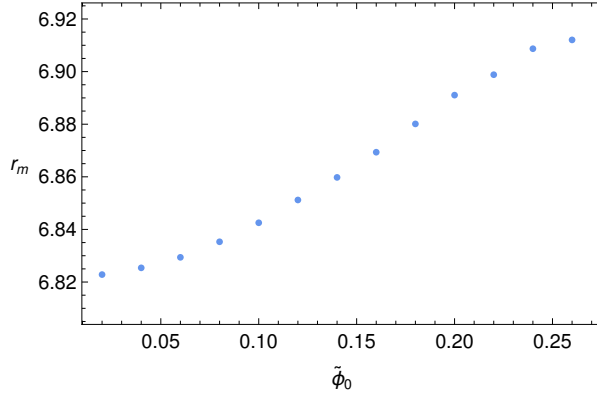


Figure 4. *Magnification due to beyond Horndeski black holes with $0 < \tilde{\phi}_0 < 0.3$. Assuming that $\tilde{\phi}_0$ is constrained to be very close to 0 by other types of observations, this would mean that the magnification r_m would be nearly indistinguishable from the magnification due to a Schwarzschild black hole.*

we use, $z = 0.997$, requires a moderate knowledge of the numerical solution, up to $x \lesssim 450$ and gives a precision of at least three decimal places in the result of I_R .

- iv. Compute c_2 from Eq. (17). Having all the previous results at hand, this step is a simple substitution into Eq. (17). The results are shown in the right panel of Fig. 3. Notice that the relative change in c_2 is one order of magnitude bigger than the change in c_1 . This is in contrast with known results for Horndeski black holes [14], and also with the case of Reissner-Nordström (e.g., [17]), where the changes in c_1 and c_2 arising from changes in the charges or parameters of each model are comparable, but is similar to results for the Janis-Newman-Winicour (JNW) naked singularity [17], where at leading order c_1 remains equal to 1 while c_2 experiences changes of order 1. However, it is possible to distinguish JNW from our beyond Horndeski solutions by the sign of the changes in c_2 : for JNW, c_2 is larger than its Schwarzschild value, while for the beyond Horndeski solutions that we study the opposite is true.

Let us close this section by analysing the observable r defined in Eq. (28). This quantity depends only on c_1 , therefore we can study it without making reference to particular masses or distances of an astrophysical system. As we discussed above, the deviations of c_1 with respect to its Schwarzschild value $c_1 = 1$ are minimal, and this is inherited to r . Fig. 4 shows $r_m = 2.5 \log_{10} r$.

5. Supermassive black holes

In the previous sections we obtained all the quantities required in order to make specific predictions for observables that could be constrained, for instance, with future data from the Event Horizon Telescope [10]. Let us focus in two astrophysical systems targeted by these observations: the supermassive black hole candidate, Sagittarius A* [45] (Sgr A*), at the center of our galaxy, and the one at the center of the giant elliptical galaxy

Table 1. Estimates for the observables s and θ_∞ defined in the text, for the supermassive black hole candidate *Sgr A**, assuming a mass $M^{Sgr} = 4.28 \times 10^6 M_\odot$ and a distance $D_{OL} = 8.32 \text{ kpc}$. For clarity we display the range $0 \leq \tilde{\phi}_0 \leq 0.14$. We remind the reader that $\tilde{\phi}_0 = 2M\phi_0$ and we have set $\tilde{g}_4 = g_4/(4M^2) = 1$.

$\tilde{\phi}_0$	0	0.02	0.04	0.06	0.08	0.10	0.12	0.14
$\theta_\infty(\mu\text{as})$	26.40	26.37	26.30	26.18	26.01	25.80	25.52	25.18
$s(\mu\text{as})$	0.0329	0.0328	0.0325	0.0321	0.0315	0.0307	0.0298	0.0288

Table 2. Estimates for the observables s and θ_∞ defined in the text, for the supermassive black hole candidate in M87, assuming a mass $M^{M87} = 6.5 \times 10^9 M_\odot$ and a distance $D_{OL} = 16.8 \text{ Mpc}$. For clarity we display the range $0 \leq \tilde{\phi}_0 \leq 0.14$. We remind the reader that $\tilde{\phi}_0 = 2M\phi_0$ and we have set $\tilde{g}_4 = g_4/(4M^2) = 1$.

$\tilde{\phi}_0$	0	0.02	0.04	0.06	0.08	0.10	0.12	0.14
$\theta_\infty(\mu\text{as})$	19.85	19.83	19.77	19.69	19.57	19.40	19.19	18.94
$s(\mu\text{as})$	0.0248	0.0247	0.0245	0.0241	0.0234	0.0231	0.0224	0.0216

M87[46].

For Sgr A* we use the central values of the observational data reported in [47]: $M^{Sgr} = 4.28 \times 10^6 M_\odot$, where M_\odot is the solar mass, and $D_{OL} = 8.32 \text{ kpc}$. Both measurements have systematic and statistical uncertainties in the order of 10^{-1} . Reintroducing the appropriate factors of the Newton constant G and the speed of light c , we have $2M = 2GM^{Sgr}/c^2 = 1.26 \times 10^{10} \text{ m}$, this is used to compute b_c from $\tilde{b}_c = b_c/2M$. Then we obtain $\theta_\infty = b_c/D_{OL}$, and finally we get s from Eq. (31). It is worth noticing the advantage of having redefined all the quantities in the metric in such a way that the mass does not appear explicitly: obtaining results for specific systems from the generic results reported in the previous section only requires introducing the appropriate values of the mass in \tilde{b}_c . The results for θ_∞ and s are shown in Table 1.

For M87 we use the central values adopted in [48]: $M = 6.5 \times 10^9 M_\odot$ and $D_{OL} = 16.8 \text{ Mpc}$. Restoring factors of G and c , this mass leads to $2M = 1.92 \times 10^{13} \text{ m}$. The values of θ_∞ and s are reported in Table 2.

The consequences of the results displayed in Tables 1 and 2 for the values of g_4 and ϕ_0 have to be interpreted with some care. We are actually using the redefined quantities \tilde{g}_4 and $\tilde{\phi}_0$, which are given in relation to the value of $2M$ for each astrophysical system, so, for instance, $\tilde{\phi}_0 = 0.02$ implies a different value of ϕ_0 for each M . Furthermore, we are fixing $\tilde{g}_4 = g_4/(4M^2) = 1$. This implies large values of g_4 , but we also have small values of ϕ_0 , so that the combination $g_4\phi_0^2$ remains natural. Indeed, as we noticed before, these parameters satisfy $g_4\phi_0^2 = \tilde{g}_4\tilde{\phi}_0^2$. If one wishes to fix $g_4 \sim 1$, a large $\tilde{\phi}_0$ – order $2M$ – would be required in order to recover values of $\tilde{g}_4\tilde{\phi}_0^2$ similar to the ones we have used, but the terms of order $1/x^2$ in the metric would still be suppressed by a factor of order M^2 , leading to smaller deviations from a Schwarzschild black hole. Considering that angular measurements from EHT have an uncertainty of about $3 \mu\text{as}$, our results show that even for a large coupling g_4 , beyond Horndeski black holes lead to lensing

observables that are compatible with current data, although could be excluded in the near future.

6. Deflection angle for large x_0

As we mentioned before, Bozza's approximation is accurate only near the photon sphere located at x_m . For light rays whose closest approach distance x_0 is away from x_m , we explore the deflection angle under a different approximation. We follow the methodology presented in [18] – later generalized in [49], where using the method introduced by Amore et al. [50] and the principle of minimal sensitivity (PMS) [51] to minimize the error, an analytical approximation for the deflection angle is obtained. This methodology, which we briefly review below, is not based on a perturbative expansion, and it describes accurately the physics of our problem almost up to the photon sphere.

Starting from Eq. (12) for the deflection angle, using a new variable $z = x_0/x$ [¶], and introducing a *potential* defined in terms of the components of the metric,

$$V(z) = \frac{z^4}{x_0^2} \left[\frac{C(\frac{x_0}{z})}{B(\frac{x_0}{z})} - \frac{C^2(\frac{x_0}{z})A(x_0)}{B(\frac{x_0}{z})A(\frac{x_0}{z})C(x_0)} \right] + x_0^2 \frac{A(x_0)}{C(x_0)}, \quad (34)$$

the deflection angle can be written as,

$$\alpha(z) = 2 \int_0^1 \frac{dz}{\sqrt{V(1) - V(z)}} - \pi, \quad (35)$$

where A, B, C are as defined in (33). A note regarding the boundary conditions is pertinent: in [18], it is assumed that $\lim_{z \rightarrow 0} C(x_0/z) = x_0^2/z^2$, while $A(z_0/z) \rightarrow 1$ and $B(z_0/z) \rightarrow 1$ in the same limit, so that $V(0) = 0$. In our case, $\lim_{z \rightarrow 0} C(x_0/z) = s_0^{-1}x_0^2/z^2$, leading to $V(0) = A(x_0)(-s_0^{-1} + s_0)$, i.e., $V(0)$ has a constant value. As we can see, this constant value cancels out in Eq. (35); however, it is important to take it into account in the analysis that we describe below.

The integral (35) can be solved analytically for particular cases, e.g., Schwarzschild [5, 52] and Reissner-Nordström [53]. For more general cases, the methodology presented in [18] allows to find an analytical approximation. Under the assumption that the metric is locally flat at infinity, the potential (34) is approximated as a power series in z ,

$$V(z) \approx V_k(z) = \sum_{n=0}^k v_n z^n, \quad (36)$$

notice that unlike [18] we are including the constant term, v_0 , in order to account correctly for the behaviour of $V(z)$ at $z = 0$, and we are already recognising that the power series may need to be truncated at some finite value k .

[¶] Notice that this is not the same z that we used in previous sections. Since the contents of these sections do not mix, we hope this is not misleading.

Using a nonperturbative method based on a Linear Delta Expansion [50, 54], Amore et al. obtain (see [18, 49] for details)

$$\alpha_{\text{PMS}}^{(1)} = \sqrt{\frac{\pi^3}{2\rho(1)}} - \pi, \quad (37)$$

where (1) indicates the order of the approximation, and $\rho(z)$ is given by

$$\rho(z) = \sqrt{\pi} \sum_{n=0}^k v_n \left(\frac{\Gamma(n/2 + 1/2)}{\Gamma(n/2)} \right) z^n, \quad (38)$$

where Γ is the Gamma function.

In some cases, such as Schwarzschild and Reissner-Nördstrom, the power series for $V(z)$ is finite, and the set of coefficients v_n can be exactly identified. In other cases, even if the metric is known analytically, the power series is not finite, and a truncation needs to be made, this happens, for instance, for the JNW metric and for Einstein-Born-Infeld black holes. In our case, the metric is not known analytically, so we need to perform a numerical fit of the potential $V(z)$ to a power series in z , which we choose to truncate at $n = 6$. Let us explain our methodology.

- First we select a value of $\tilde{\phi}_0$, then we construct $V(z)$ from Eq. (34) using the numerical solutions for the metric corresponding to this $\tilde{\phi}_0$. Since $V(z)$ takes x_0 as a parameter, for each $\tilde{\phi}_0$ we get a set of profiles for $V(z)$, each one associated to a value of x_0 in the range $x_m < x_0 \lesssim 50$, with x_m computed from Eq. (11). Notice that x_0/z cannot be larger than the maximum x for which the numerical solution is known, so, an upper limit on x_0 translates into a lower limit in z . Now, for each x_0 , we fit the numerical profile of $V(z)$ to a power series in z truncated at $k = 6$, $V_6(z)$. Figure 5 shows the results for $\tilde{\phi}_0 = 0.02$, with $x_0 = x_m$. The relative percentage error of the numerical fit, $|V_k(z) - V(z)|/V(z) \times 100\%$, stays below 1%.
- With the coefficients v_i at hand, we use Eqs. (37) and (38) to compute the deflection angle for each x_0 .

We repeat the steps above for different values of $\tilde{\phi}_0$ in the range $0 \leq \tilde{\phi}_0 \leq 0.32$. Fig. 6 shows the deflection angle as a function of x_0 for different choices of $\tilde{\phi}_0$. As we can observe, $\tilde{\phi}_0$ – or $\tilde{g}_4\tilde{\phi}_0^2$ as we infer from the angular part of the metric – modifies the asymptotic behavior of the deflection angle, making it negative for sufficiently large x_0 . A negative deflection angle indicates a divergent lens, this has been reported in [55, 56, 57, 58] for wormholes and massless braneworld black holes. In [59, 60] some consequences of negative deflection angles are discussed.

Phenomenologically, the weak field deflection angle is constrained by Solar System observations (e.g., VLBI [2]) to be within $\sim 10^{-4}$ of the GR prediction. This would imply a tight constraint on $\tilde{g}_4\tilde{\phi}_0^2$, but we need to remember that $\tilde{\phi}_0$ is a parameter of the solution, not of the model, so it might well be different in different astrophysical scales. Similarly, no gravitational, divergent deflection angle has been reported in flat space. These observations indicate that in the weak field limit, $g_4\phi_0^2 = \tilde{g}_4\tilde{\phi}_0^2 \rightarrow 0$. Recalling the

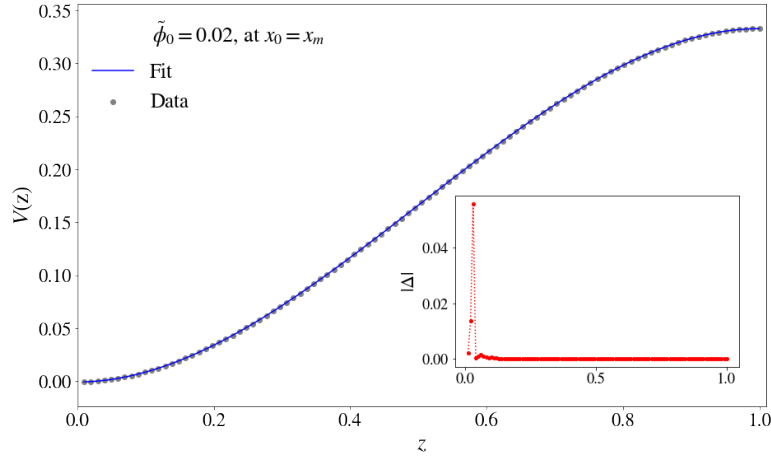


Figure 5. Comparison between the approximated potential $V_6(z)$ and the full numerical profile $V(z)$. The inset shows the relative percentage error $|\Delta| = |\bar{V}(z) - V(z)| / V(z) \times 100\%$. In this plot we use $\tilde{\phi}_0 = 0.02$, with the potential computed for a light ray whose minimum distance approach is $x_0 = x_m$. For larger $\tilde{\phi}_0$, up to 0.32, $|\Delta|$ grows, but stays below 1%.

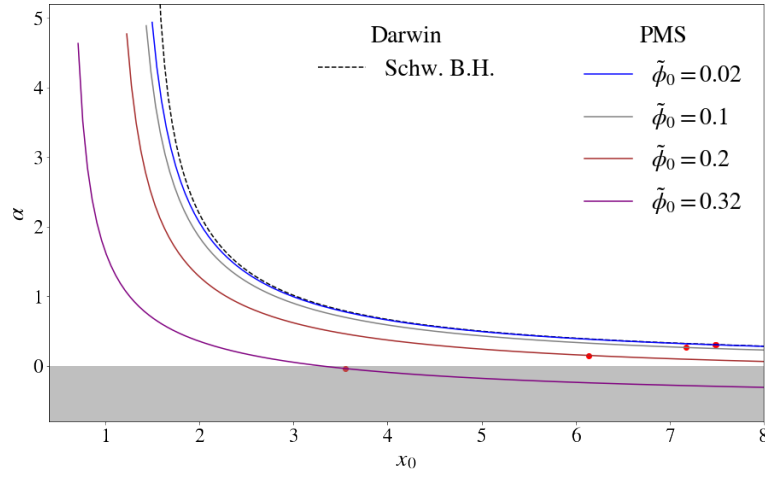


Figure 6. Deflection angle as a function of x_0 . The dashed line corresponds to the exact result for Schwarzschild (Darwin, [5, 52]), while the others are for $\tilde{\phi}_0 \neq 0$ using the PMS approximation. As $\tilde{\phi}_0$ increases, α deviates non-linearly from its Schwarzschild value. To exemplify this, we show (red dots) the deflection angle for $x_0 = 5x_m$ for each $\tilde{\phi}_0$. The fact that α becomes negative is discussed in the main text.

results of the previous section, there is still the possibility that in strong field regimes, $g_4\phi_0^2 \sim 10^{-1}$.

Given that the asymptotic deflection angle is controlled by the angular part of the metric (33), it is possible to use a further analytical approximation upon the PMS first order result by replacing Eq. (33) with a Schwarzschild metric, but with the angular

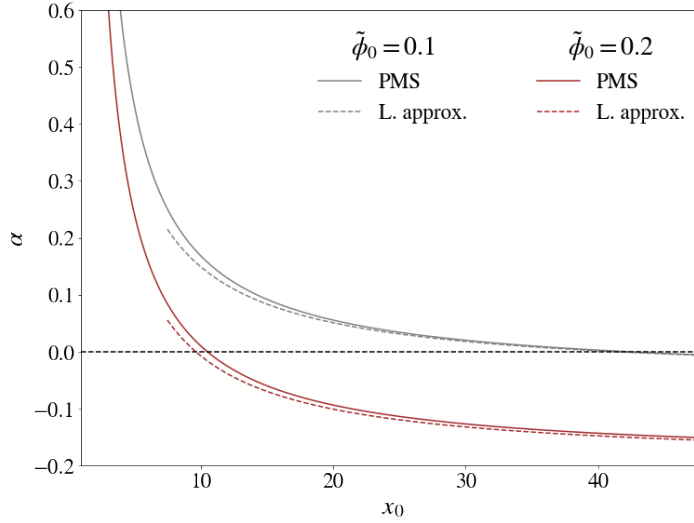


Figure 7. Comparison between the PMS-analytic (L. approx., Eq. (40), dashed lines) and the PMS-numerical approaches (solid lines) for $\tilde{\phi}_0 = 0.1$ and $\tilde{\phi}_0 = 0.2$. For large values of x_0 both approximations are consistent.

component rescaled by s_0^{-1} . Following [18], this approach leads to

$$\alpha_{\text{PMS}}^{(1)} = \pi \left(\frac{\sqrt{s_0}}{\sqrt{1 - \frac{4}{\pi x_0}}} - 1 \right). \quad (39)$$

We remind the reader that $s_0 = 1 - 3\tilde{g}_4\tilde{\phi}_0^2$. If $x_0 \gg 1$, we can write

$$\alpha_{\text{PMS}}^{(1)} \approx \pi (\sqrt{s_0} - 1) + \frac{2\sqrt{s_0}}{x_0}. \quad (40)$$

Notice that for $s_0 = 0$ the weak field GR deflection angle is recovered. Figure 7 shows that this analytical approach is consistent with the results of a numerical PMS approximation.

To conclude this section, let us put together the two numerical methods to compute the deflection angle presented so far. In Bozza's approximation, we can obtain the deflection angle for a given x_0 with the help of Eqs. (14) and (15). The results are shown in Fig. (8) for Schwarzschild and for $\tilde{\phi}_0 = 0.2$. On the other hand, using the PMS method described in this section, we can also obtain the deflection angle for a given x_0 , the results are shown in the same figure. As expected, these approximations disagree close to the photon sphere and also for large distances. However, it is interesting to note that, together, they describe accurately the deflection angle over all the range of x_0 : when Bozza's approximation begins to fail, the PMS method starts to give good results. To see this, we include in Fig. (8) the exact solution for Schwarzschild, and a full numerical result for $\tilde{\phi}_0 = 0.2$ obtained by direct integration of Eq. (12). It is worth mentioning that direct integration is more computationally expensive than the numerical implementation of Bozza's method: for each $\tilde{\phi}_0$, Bozza's method reduces to

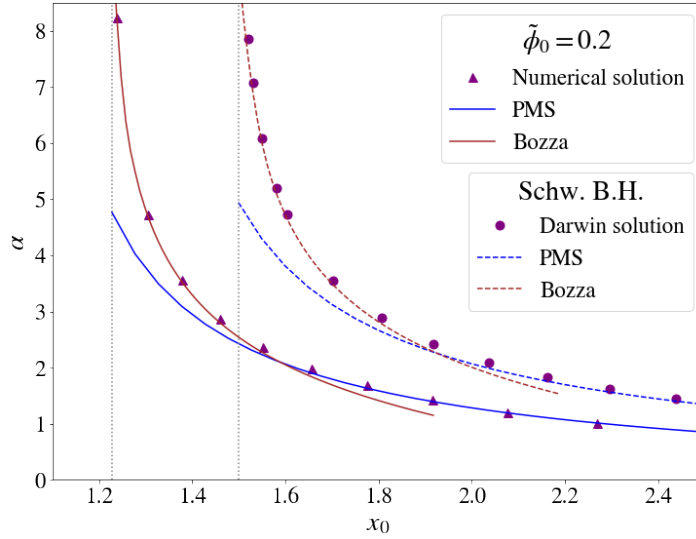


Figure 8. *Reconstruction of exact or full-numerical deflection angles as the union of the hybrid Bozza-numerical and PMS-numerical approximations. The red triangles/circles are the full numerical/analytical deflection angles for $\tilde{\phi}_0 = 0.2$ /Schwarzschild. Jumping from one approximation to the other at their intersection (roughly $x_0 \approx 1.4x_m$) the exact results are accurately described. The vertical dotted line indicates x_m .*

computing only one integral, while a full numerical result requires one integral for each x_0 .

7. Discussion

Gravitational deflection of light is an important test for modified theories of gravity. Here we have focused on models that fit within the DHOST category of modified gravity. Thanks to screening mechanisms, some of these theories admit an exact Schwarzschild solution, thus automatically recovering the basic predictions of GR for weak and strong deflection of light. However, on general grounds, the DHOST Lagrangian may contain terms that lead to modifications of the Schwarzschild metric, and in many cases to solutions that cannot be obtained in exact form but only under some approximations or numerical treatment. In this work we studied one of these models, which besides modifying the radial and time components of the Schwarzschild metric, also modifies the angular part.

The deflection angle in the strong field limit is given by an integral that diverges at the photon sphere, and that can be solved analytically only in a few cases. This motivated the development of strong field approximations. In particular, Bozza's approximation has two advantages that are relevant for our work: first, it is given in terms of coefficients that are directly related to observables, second, the same set of coefficients – that depend on one integral – is accurate over a certain interval for x_0 away from the photon sphere. Numerically, we could integrate the exact expression for

the deflection angle, but this can be quite inefficient, since one integral is required for each closest approach distance x_0 that we want to investigate.

In view of the above, we investigated a hybrid analytic-numerical method based on Bozza's approach. In the Schwarzschild limit, we verified that our results near the photon sphere agree with exact and fully analytic approximations. For the non-Schwarzschild solutions of the DHOST model we consider, we compared our results to full numerical integration, finding good agreement as well. These results are relevant not only because they show that a hybrid method is a good replacement for full integration, but also because this method can be used for static, spherically symmetric solutions that are known only numerically. In this spirit, we also investigated a hybrid method to compute the deflection angle away from the photon sphere, this time with the analytic part based on the PMS approach. We verified that for $x_0 \gtrsim 1.5 x_m$, this method is consistent with exact or full numerical results. In summary, we have shown that it is possible to compute the deflection angle (12) over the entire range of x_0 as the union of two hybrid approximations,

$$\alpha(x_0) = \begin{cases} \text{Bozza-numerical approach} & \text{for } x_m \lesssim x_0 \lesssim 1.5 x_m \\ \text{PMS-numerical approach} & \text{for } x_0 \gtrsim 1.5 x_m. \end{cases} \quad (41)$$

Furthermore, we have shown that for $x_0 \gtrsim 20 x_m$, an analytic weak field approximation based on the Schwarzschild metric with a rescaled angular component correctly accounts for the effects of a constant angular deficit in the metric.

Regarding the phenomenology of the DHOST model we consider in this work, using the strong deflection results we calculated the angular position θ_∞ where lensed images accumulate around a supermassive black hole, as well as the separation s between these images and the outermost one. Specifically, we considered Sagittarius A* and M87, finding that, for the range of parameters that we use, the deviations of θ_∞ from its Schwarzschild value are in the order of micro arc seconds. Current observations by EHT constrain the angular diameter of M87's shadow with an uncertainty of $\pm 3 \mu\text{as}$. In the near future, this type of observations could impose constraints on non-perfectly screened modified gravity black holes at order 10^{-1} in the relative size of the corrections. Although this is weaker than the constraints in the Solar System – order 10^{-4} , strong deflection tests a completely different regime of the theory and provides complementary information that can be used to further reduce the space of viable modified gravity models.

Acknowledgments

A.R. and B.R. acknowledge support by CONACyT graduate scholarships No. 570326 and No. 733442.

References

- [1] Ellis R S 2010 *Philosophical transactions. Series A, Mathematical, physical, and engineering sciences* **368** 967 – 987
- [2] Shapiro S, Davis J, Lebach D and Gregory J 2004 *Phys. Rev. Lett.* **92** 121101
- [3] Schmidt F 2008 *Physical Review D* **78** ISSN 1550-2368 URL <http://dx.doi.org/10.1103/PhysRevD.78.043002>
- [4] Pratten G, Munshi D, Valageas P and Brax P 2016 *Physical Review D* **93** ISSN 2470-0029 URL <http://dx.doi.org/10.1103/PhysRevD.93.103524>
- [5] Darwin C G 1959 *Proceedings of the Royal Society of London. Series A. Mathematical and Physical Sciences* **249** 180–194 (Preprint <https://royalsocietypublishing.org/doi/pdf/10.1098/rspa.1959.0015>) URL <https://royalsocietypublishing.org/doi/abs/10.1098/rspa.1959.0015>
- [6] Cunningham C T and Bardeen J M 1972 *ApJ* **173** L137
- [7] Luminet J P 1979 *AA* **75** 228–235
- [8] Falcke H, Melia F and Agol E 2000 *ApJ* **528** L13–L16 (Preprint [astro-ph/9912263](https://arxiv.org/abs/astro-ph/9912263))
- [9] Doeleman S *et al.* 2001 *Astron. J.* **121** 2610 (Preprint [astro-ph/0102232](https://arxiv.org/abs/astro-ph/0102232))
- [10] Akiyama K *et al.* (Event Horizon Telescope) 2019 *Astrophys. J.* **875** L1 (Preprint [1906.11238](https://arxiv.org/abs/1906.11238))
- [11] Virbhadra K, Narasimha D and Chitre S 1998 *Astron. Astrophys.* **337** 1–8 (Preprint [astro-ph/9801174](https://arxiv.org/abs/astro-ph/9801174))
- [12] Wei S W, Yang K and Liu Y X 2015 *The European Physical Journal C* **75** ISSN 1434-6052 URL <http://dx.doi.org/10.1140/epjc/s10052-015-3469-7>
- [13] Zhao S S and Xie Y 2016 *JCAP* **07** 007 (Preprint [1603.00637](https://arxiv.org/abs/1603.00637))
- [14] Badía J and Eiroa E F 2017 *Eur. Phys. J. C* **77** 779 (Preprint [1707.02970](https://arxiv.org/abs/1707.02970))
- [15] Izmailov R, Karimov R, Zhdanov E and Nandi K 2019 *Mon. Not. Roy. Astron. Soc.* **483** 3754–3761 (Preprint [1905.01900](https://arxiv.org/abs/1905.01900))
- [16] Xu C and Yang Y 2018 *J. Math. Phys.* **59** 032501 (Preprint [1709.04127](https://arxiv.org/abs/1709.04127))
- [17] Bozza V 2002 *Physical Review D* **66** ISSN 1089-4918 URL <http://dx.doi.org/10.1103/PhysRevD.66.103001>
- [18] Amore P and Arceo S 2006 *Phys. Rev. D* **73**(8) 083004 URL <https://link.aps.org/doi/10.1103/PhysRevD.73.083004>
- [19] Zumalacárregui M and García-Bellido J 2014 *Physical Review D* **89** ISSN 1550-2368 URL <http://dx.doi.org/10.1103/PhysRevD.89.064046>
- [20] Gleyzes J, Langlois D, Piazza F and Vernizzi F 2015 *Physical Review Letters* **114** ISSN 1079-7114 URL <http://dx.doi.org/10.1103/PhysRevLett.114.211101>
- [21] Horndeski G W 1974 *Int. J. Theor. Phys.* **10** 363–384
- [22] Woodard R P 2015 *Scholarpedia* **10** 32243 (Preprint [1506.02210](https://arxiv.org/abs/1506.02210))
- [23] Langlois D and Noui K 2016 *Journal of Cosmology and Astroparticle Physics* **2016** 034034 ISSN 1475-7516 URL <http://dx.doi.org/10.1088/1475-7516/2016/02/034>
- [24] Achour J B, Crisostomi M, Koyama K, Langlois D, Noui K and Tasinato G 2016 *Journal of High Energy Physics* **2016** ISSN 1029-8479 URL [http://dx.doi.org/10.1007/JHEP12\(2016\)100](http://dx.doi.org/10.1007/JHEP12(2016)100)
- [25] Crisostomi M, Koyama K and Tasinato G 2016 *Journal of Cosmology and Astroparticle Physics* **2016** 044044 ISSN 1475-7516 URL <http://dx.doi.org/10.1088/1475-7516/2016/04/044>
- [26] Clifton T, Ferreira P G, Padilla A and Skordis C 2012 *Physics Reports* **513** 1189 ISSN 0370-1573 URL <http://dx.doi.org/10.1016/j.physrep.2012.01.001>
- [27] Cisterna A, Delsate T and Rinaldi M 2015 *Physical Review D* **92** ISSN 1550-2368 URL <http://dx.doi.org/10.1103/PhysRevD.92.044050>
- [28] Babichev E, Koyama K, Langlois D, Saito R and Sakstein J 2016 *Classical and Quantum Gravity* **33** 235014 ISSN 1361-6382 URL <http://dx.doi.org/10.1088/0264-9381/33/23/235014>
- [29] Babichev E, Charmousis C and Lehébel A 2016 *Classical and Quantum Gravity* **33** 154002 ISSN 1361-6382 URL <http://dx.doi.org/10.1088/0264-9381/33/15/154002>

- [30] Maselli A, Silva H O, Minamitsuji M and Berti E 2016 *Physical Review D* **93** ISSN 2470-0029 URL <http://dx.doi.org/10.1103/PhysRevD.93.124056>
- [31] Babichev E, Charmousis C and Lehébel A 2017 *Journal of Cosmology and Astroparticle Physics* **2017** 027027 ISSN 1475-7516 URL <http://dx.doi.org/10.1088/1475-7516/2017/04/027>
- [32] Chagoya J and Tasinato G 2018 *Journal of Cosmology and Astroparticle Physics* **2018** 006006 ISSN 1475-7516 URL <http://dx.doi.org/10.1088/1475-7516/2018/08/006>
- [33] Kobayashi T and Hiramatsu T 2018 *Physical Review D* **97** ISSN 2470-0029 URL <http://dx.doi.org/10.1103/PhysRevD.97.104012>
- [34] Abbott B *et al.* (LIGO Scientific, Virgo, Fermi-GBM, INTEGRAL) 2017 *Astrophys. J. Lett.* **848** L13 (*Preprint* [1710.05834](https://arxiv.org/abs/1710.05834))
- [35] Abbott B, Abbott R, Abbott T, Acernese F, Ackley K, Adams C, Adams T, Addesso P, Adhikari R, Adya V and *et al* 2017 *Physical Review Letters* **119** ISSN 1079-7114 URL <http://dx.doi.org/10.1103/PhysRevLett.119.161101>
- [36] Ezquiaga J M and Zumalacárregui M 2017 *Phys. Rev. Lett.* **119** 251304 (*Preprint* [1710.05901](https://arxiv.org/abs/1710.05901))
- [37] Deffayet C, Gao X, Steer D A and Zahariade G 2011 *Physical Review D* **84** ISSN 1550-2368 URL <http://dx.doi.org/10.1103/PhysRevD.84.064039>
- [38] Kobayashi T, Yamaguchi M and Yokoyama J 2011 *Progress of Theoretical Physics* **126** 511529 ISSN 1347-4081 URL <http://dx.doi.org/10.1143/PTP.126.511>
- [39] Kobayashi T, Watanabe Y and Yamauchi D 2015 *Physical Review D* **91** ISSN 1550-2368 URL <http://dx.doi.org/10.1103/PhysRevD.91.064013>
- [40] Koyama K and Sakstein J 2015 *Phys. Rev. D* **91** 124066 (*Preprint* [1502.06872](https://arxiv.org/abs/1502.06872))
- [41] Weinberg S 1972 *Gravitation and Cosmology: Principles and Applications of the General Theory of Relativity* (New York, NY: Wiley) URL <https://cds.cern.ch/record/100595>
- [42] Tsukamoto N 2017 *Physical Review D* **95** ISSN 2470-0029 URL <http://dx.doi.org/10.1103/PhysRevD.95.064035>
- [43] Man J, Wang H and Cheng H 2010 The strong field gravitational lensing in the schwarzschild black hole pierced by a cosmic string (*Preprint* [1010.2308](https://arxiv.org/abs/1010.2308))
- [44] Bozza V, Capozziello S, Iovane G and Scarpetta G 2001 *General Relativity and Gravitation* **33** 15351548 ISSN 1572-9532 URL <http://dx.doi.org/10.1023/A:1012292927358>
- [45] Eckart A and Genzel R 1997 *Mon. Not. Roy. Astron. Soc.* **284** 576–598
- [46] Gebhardt K, Adams J, Richstone D, Lauer T R, Faber S M, Gültekin K, Murphy J and Tremaine S 2011 *The Astrophysical Journal* **729** 119 ISSN 1538-4357 URL <http://dx.doi.org/10.1088/0004-637X/729/2/119>
- [47] Gillessen S, Plewa P M, Eisenhauer F, Sari R, Waisberg I, Habibi M, Pfuhl O, George E, Dexter J, Fellenberg S *v* and *et al* 2017 *The Astrophysical Journal* **837** 30 ISSN 1538-4357 URL <http://dx.doi.org/10.3847/1538-4357/aa5c41>
- [48] Akiyama K *et al.* (Event Horizon Telescope) 2019 *Astrophys. J. Lett.* **875** L6 (*Preprint* [1906.11243](https://arxiv.org/abs/1906.11243))
- [49] Amore P, Arceo S and Fernández F M 2006 *Phys. Rev. D* **74**(8) 083004 URL <https://link.aps.org/doi/10.1103/PhysRevD.74.083004>
- [50] Amore P and Sáenz R A 2005 *Europhysics Letters (EPL)* **70** 425–431
- [51] Stevenson P M 1981 *Phys. Rev. D* **23**(12) 2916–2944 URL <https://link.aps.org/doi/10.1103/PhysRevD.23.2916>
- [52] Darwin C G 1961 *Proceedings of the Royal Society of London. Series A. Mathematical and Physical Sciences* **263** 39–50 (*Preprint* <https://royalsocietypublishing.org/doi/pdf/10.1098/rspa.1961.0142>) URL <https://royalsocietypublishing.org/doi/abs/10.1098/rspa.1961.0142>
- [53] Eiroa E F, Romero G E and Torres D F 2002 *Phys. Rev. D* **66**(2) 024010 URL <https://link.aps.org/doi/10.1103/PhysRevD.66.024010>
- [54] Amore P, Aranda A, Sáenz R and Fernández F M 2005 *Phys. Rev. E* **71**(1) 016704 URL <https://link.aps.org/doi/10.1103/PhysRevE.71.016704>

- [55] Cramer J G, Forward R L, Morris M S, Visser M, Benford G and Landis G A 1995 *Phys. Rev. D* **51** 3117–3120 (*Preprint* [astro-ph/9409051](#))
- [56] Shaikh R and Kar S 2017 *Phys. Rev. D* **96** 044037 (*Preprint* [1705.11008](#))
- [57] Shaikh R and Kar S 2016 *Phys. Rev. D* **94** 024011 (*Preprint* [1604.02857](#))
- [58] Eiroa E F and Sendra C M 2012 *Phys. Rev. D* **86** 083009 (*Preprint* [1207.5502](#))
- [59] Izumi K, Hagiwara C, Nakajima K, Kitamura T and Asada H 2013 *Phys. Rev. D* **88** 024049 (*Preprint* [1305.5037](#))
- [60] Kitamura T, Nakajima K and Asada H 2013 *Phys. Rev. D* **87** 027501 (*Preprint* [1211.0379](#))